Attenuation of DNA Replication by HIV-1 Reverse Transcriptase near the Central Termination Sequence†

Michael E. Ignatov,‡ Anthony J. Berdis,*,§ Stuart F. J. Le Grice,|| and Mary D. Barkley*,‡

Departments of Chemistry and Pharmacology, Case Western Reserve University, 10900 Euclid Avenue, Cleveland, Ohio 44106, and HIV Drug Resistance Program, National Cancer Institute—Frederick, Frederick, Maryland 21702

Received September 16, 2004; Revised Manuscript Received December 7, 2004

ABSTRACT: Previous pre-steady-state kinetic studies of equine infectious anemia virus-1 (EIAV) reverse transcriptase (RT) showed two effects of DNA substrates containing the central termination sequence (CTS) on the polymerization reaction: reduction of burst amplitude in single nucleotide addition experiments and accumulation of termination products during processive DNA synthesis [Berdis, A. J., Stetor, S. R., Le Grice, S. F. J., and Barkley, M. D. (2001) *Biochemistry 40*, 12140−12149]. The present study of HIV RT uses pre-steady-state kinetic techniques to evaluate the molecular mechanisms of the lower burst amplitudes using both random sequence and CTS-containing DNA substrates. The effects of various factors, including primer/template length, binding orientation, and protein concentration, on the burst amplitude were determined using random sequence DNA substrates. The percent active RT increases with total RT concentration, indicating that reversible dissociation of RT dimer is responsible for substoichiometric burst amplitudes with normal substrates. This finding was confirmed by gel mobility shift assays. Like EIAV RT, HIV RT showed lower burst amplitudes on CTS-containing DNA substrates compared to random sequences. The dissociation kinetics of RT−DNA complexes were monitored by enzyme activity and fluorescence. Biphasic kinetics were observed for both random sequence and CTS-containing DNA complexes, revealing two forms of the RT−DNA complex. A mechanism is proposed to account for reduction in burst amplitude of CTS-containing DNA that is consistent with the results of both single nucleotide addition and dissociation experiments. The two forms of the RT−DNA complex may represent partitioning of primer/template between the P- and N-sites on RT for the nucleic acid substrate.

HIV-1[1] reverse transcriptase is a versatile enzyme that synthesizes double-stranded proviral DNA from single-stranded viral RNA. In the process, RT catalyzes both RNA- and DNA-dependent DNA polymerization and RNase H hydrolysis. The native enzyme in the virion is a heterodimer of p66 and p51 subunits (*1*). The p66 subunit has polymerase and RNase H domains. The p51 subunit is derived from p66 by proteolytic removal of the C-terminal RNase H domain. A dimeric enzyme form is requisite for enzyme activity. The p66/p51 heterodimer and p66/p66 homodimer have both polymerase and RNase H activities (*2*, *3*); the p51/p51 homodimer has only polymerase activity (*2*, *4*). The heterodimer has an asymmetric structure with a single polymerase active site on the p66 subunit (*5*, *6*). In addition to RT, several *cis*-acting sequences on the nucleic acid orchestrate key steps in HIV-1 replication. These include the primer binding site, long terminal repeats, 3′ and central polypurine tracts, and central termination sequence. The CTS is a 29 bp sequence with weak and strong termination sites for (+) strand DNA synthesis (*7*).

The DNA polymerization reaction has been extensively studied by steady-state and pre-steady-state kinetic techniques. Like other DNA polymerases, RT obeys an ordered mechanism with sequential addition of substrates and elimination of products (*8*). Scheme 1 shows a minimal kinetic mechanism, where E is RT and $D_{n,n+1}$ is primer/template. More detailed mechanisms include an enzyme conformational change in the ternary $E{\cdot}D_n{\cdot}$dNTP complex before the chemical step (*9*, *10*). The rate-limiting step for enzyme turnover is attributed to slow dissociation of $E{\cdot}D_{n+1}$, because $k_{cat} = k_{off}$ (*9*−*11*). The time course of single nucleotide addition has a rapid initial burst phase followed by a slow linear steady-state phase. The amplitude of the burst phase at saturating concentration of DNA substrate is commonly taken to be the amount of catalytically active enzyme. RT is often reported to be less than 100% active (*9*, *10*, *12*−*16*). The source of the substoichiometric burst amplitudes remains a matter of ongoing debate (*17*, *18*). The

† This work was supported by NIH Grant GM52263.

* To whom correspondence should be addressed. A.J.B.: tel, (216) 368-4723; fax, (216) 368-3395; e-mail, ajb15@case.edu. M.D.B.: tel, (216) 368-0602; fax, (216) 368-0604; e-mail, mdb4@case.edu.

‡ Department of Chemistry, Case Western Reserve University.

§ Department of Pharmacology, Case Western Reserve University.

|| National Cancer Institute—Frederick.

[1] Abbreviations: BSA, bovine serum albumin; CTS, central termination sequence; dNTP, deoxynucleoside 5′-triphosphate; DTT, dithiothreitol; EDTA, ethylenediaminetetraacetic acid; EIAV, equine infectious anemia virus-1; HIV-1, human immunodeficiency virus type 1; KF, Klenow fragment of DNA polymerase I; LB, Luria broth; 6-MI, 6-methylisoxanthopterin; PBS, Dulbecco's phosphate-buffered salt solution; PP_i, pyrophosphate; PR, protease; RT, reverse transcriptase; SDS−PAGE, sodium dodecyl sulfate−polyacrylamide gel electrophoresis; gp43exo⁻, T4 DNA polymerase exo⁻; T7⁻, T7 DNA polymerase exo⁻; Tris, tris(hydroxymethyl)aminomethane.

10.1021/bi048000p CCC: $30.25
Published on Web 03/12/2005

Scheme 1: Simplified Reaction Mechanism of DNA Polymerization Catalyzed by RT

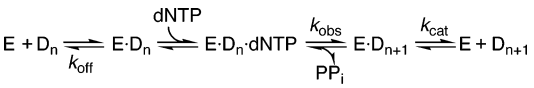

burst amplitude also appears to depend on DNA sequence (*17*, *19*).

In our previous study of DNA synthesis termination by EIAV RT (*20*), the enzyme was 50% active in single nucleotide addition experiments using DNA substrates of random sequence. For comparison, HIV-1 RT was 60% active, whereas Klenow fragment was fully active using random sequence DNA substrate. However, all three polymerases gave about 50% reduction in burst amplitude using DNA substrates containing the EIAV CTS region compared to random sequences. Because the single nucleotide addition experiments used saturating concentrations of DNA substrate, the reduced burst amplitudes were not attributable to differences in EIAV RT binding affinity for CTS-containing and random sequence DNAs. The duplex region of primer/template immediately upstream of the CTS appeared to be responsible for the apparent decrease in percent active RT. In contrast, gp43exo$^-$ was fully active using both random sequence and EIAV CTS-containing DNA substrates (unpublished data). The present study addresses two questions using HIV-1 RT. First, why were the two reverse transcriptases, but not KF and gp43exo$^-$, partially inactive on random sequence DNA substrates? We evaluate several possible reasons for this loss of RT activity, by varying reaction conditions, DNA substrate, and total RT concentration in single nucleotide addition experiments. The results indicate that substoichiometric burst amplitudes with normal substrates are due to reversible dissociation of RT dimers. We then consider the DNA sequence dependence of the burst amplitude. Namely, why did the two reverse transcriptases and KF, but not gp43exo$^-$, give reduced burst amplitudes on EIAV CTS-containing DNA substrates compared to random sequence? We measure dissociation kinetics of RT−DNA complexes in trap-chase and stopped-flow experiments using random sequence and CTS-containing DNA substrates. Biphasic dissociation kinetics are observed for all DNA substrates, which have not been reported previously. A modified kinetic mechanism is proposed for the polymerization reaction catalyzed by RT and presumably also KF. The implications of this mechanism for DNA replication are discussed.

EXPERIMENTAL PROCEDURES

Materials. Oligodeoxyribonucleotides were purchased from Operon Technologies (Alameda, CA). 6-Methylisoxanthopterin-substituted oligodeoxyribonucleotide was obtained from TriLink BioTechnologies (San Diego, CA). dCTP (>99% purity) was from Pharmacia (Peapack, NJ). [γ-^{32}P]ATP and [α-^{32}P]dCTP were from ICN Biomedicals (Irvine, CA); [γ-^{33}P]ATP was from PerkinElmer Life Sciences (Boston, MA). PBS was from Mediatech (Herndon, VA). Heparin and salmon sperm DNA were from Sigma (St. Louis, MO). Other reagents were purchased from Fisher Scientific and Roche Molecular Biochemicals. RT buffer D is 0.05 M Tris-HCl (RNase, DNase-free), pH 7.0, 25 mM NaCl, 1 mM EDTA, and 10% (v/v) glycerol (molecular grade redistilled). RT storage buffer D is RT buffer D but containing 50% (v/v) glycerol. RT reaction buffer is 0.05 M Tris-HCl, pH 7.8, 0.01 M $MgCl_2$, 0.08 M KCl, and 5 mM DTT. TE buffer is 0.01 M Tris-HCl, pH 8.0, and 1 mM EDTA.

Reverse Transcriptase. Recombinant HIV-1 RT was purified and stored at −20 °C in RT storage buffer D as described (*21*). Most experiments used the p66/p51 heterodimer with N-terminal hexahistidine extensions produced from plasmid p6H RT-PR. A few experiments used authentic p66/p51 without the His tags produced from pRT AUTH-PR. Stock solutions of 10 μM RT in RT buffer D containing 5 mM DTT were prepared by overnight dialysis at 4 °C and stored at −20 °C. Protein concentration was determined from absorbance at 280 nm. The extinction coefficient ϵ of the RT heterodimer was determined using quantitative amino acid analysis. Briefly, duplicate samples of p66/p51 were dialyzed overnight at 4 °C into PBS containing 3% glycerol and 1 mM EDTA. After the absorption spectrum was recorded, 5 μL aliquots were removed and dried in 10 × 75 mm Pyrex tubes in a SpeedVac 1100 (Savant, Holbrook, NY) for 5 h. Protein concentration was measured by amino acid analysis in the W. M. Keck Facility, Yale University School of Medicine. The experimental value of $\epsilon(280) = (2.6 \pm 0.2) \times 10^5$ M^{-1} cm^{-1} for p66/p51 is in excellent agreement with the calculated values based on amino acid composition: $\epsilon(280) = 252383$ M^{-1} cm^{-1} in 0.1 M phosphate buffer, pH 7.1 (*22*), and $\epsilon(280) = 260450$ M^{-1} cm^{-1} in 0.2 M phosphate buffer, pH 6.5, and 6 M guanidinium chloride (*23*).

gp43exo$^-$. The exonuclease-deficient form of gp43 (D219A mutant) was purified as described (*24*, *25*). The protein was >96% pure based on SDS−PAGE. Protein concentration was determined from absorbance at 280 nm, using $\epsilon(280) = 148000$ M^{-1} cm^{-1} calculated from amino acid composition (*23*). Active site titrations were performed as described to validate the concentration of active polymerase (*24*).

DNA Substrates. Synthetic oligonucleotides (see Table 1) were purified as described (*26*). DNA concentrations were determined from absorbance at 260 nm in TE buffer. Extinction coefficients for single-stranded DNAs were calculated by the nearest neighbor method (*27*). Primer/template duplexes were annealed and purified (*26*). The amount of accessible primer 3′-OH was assayed by enzymatic incorporation of [α-^{32}P]dCTP for 5−10 min (*28*). Extinction coefficients for duplex substrates were calculated by summing $\epsilon(260)$ values for single- and double-stranded regions of the DNA. The $\epsilon(260)$ for the double-stranded region was calculated by summing $\epsilon(260)$ values for the two strands assuming 26% hypochromic effect. The following extinction coefficients were used for primer/template duplexes: 25/36-mer and 25/36-mer 6-MI, $\epsilon(260) = 441900$ M^{-1} cm^{-1}; 34/62-mer, $\epsilon(260) = 764200$ M^{-1} cm^{-1}; 33/41-mer, $\epsilon(260) = 551900$ M^{-1} cm^{-1}; 30/60-mer HIV, $\epsilon(260) = 736900$ M^{-1} cm^{-1}; 30/60-mer EIAV, $\epsilon(260) = 730500$ M^{-1} cm^{-1}; and 33/41-mer HIV, $\epsilon(260) = 573500$ M^{-1} cm^{-1}. Duplex substrates were 5′-^{32}P-end labeled as described (*26*).

Pre-Steady-State Kinetics. Rapid-quench experiments were done on a KinTek RQF-3 rapid-mixing apparatus (State College, PA) as described (*29*). All kinetic experiments were carried out in RT reaction buffer. Reagent concentrations are final concentrations after 2-fold dilution into the reaction

Table 1: DNA Substrates[a]

name	sequence
25/36-mer	5′-GCCTCGCAGCCGTCCAACCAACTCA-3′ 3′-CGGAGCGTCGGCAGGTTGGTTGAGTGCGTCATGTTT-5′
25/36-mer 6MI[b]	5′-GCCTCGCAGCCGTCCAACCAACTCA-3′ 3′-CGGAGCGTCGGCAGGTTGGTTGAGT*CGTCATGTTT-5′
34/62-mer	5'-ACTCCTTCCCGCACTAATTTTTGACGCACGTTGT-3' 3'-TGAGGAAGGGCGTGATTAAAAACTGCGTGCAACAGACTACGCAGTACTATCATGCAGACACA-5'
33/41-mer	5'-TTGCTTCCCGCACTAATTTTTGACGCACGTTGT-3' 3'-GAAGGGCGTGATTAAAAACTGCGTGCAACAGCGTCATGTTT-5'
30/60-mer EIAV[c]	5'-GAAACTTTTACTACAGCAAGCACAATCCTC-3' 3'-CTTTGAAAATGATGTCGTTCGTGTTAGGAGGTTTTTTAAAACAAAAATGTTTTAGGGACC-5'
30/60-mer HIV[d]	5'-ATAGCAACAGACATACAAACTAAAGAATTA-3' 3'-TATCGTTGTCTGTATGTTTGATTTCTTAATGTTTTTGTTTAATGTTTTTAAGTTTTAAAA-5'
33/41-mer HIV	5'-TTTGTACTGCGATAGCAACAGACATACAAACTAAAGAATTA-3' 3'-TATCGTTGTCTGTATGTTTGATTTCTTAATGTT-5'

[a] Identical sequences are color coded. Gray boxes represent CTS sequences with termination sites in red. [b] The green asterisk denotes the position of the 6-MI fluorescent label. [c] The T in red = *ter*1; the A in red = *ter*2. [d] The T in red = *ter*0; the internal A in red = *ter*1; the terminal A in red = *ter*2.

mixture. RT concentration is expressed as the heterodimer and given as total protein concentration $[RT]_{tot}$ determined by absorbance at 280 nm. Reaction conditions were pseudo first order with ^{32}P-labeled DNA in excess of active polymerase.[2] Data were fit to kinetic equations using Origin 6 (Microcal Software, Inc.) or Kaleidagraph (Synergy Software).

(A) Single Nucleotide Addition. In the standard experiment, 300 nM total RT was preincubated overnight with 400 nM DNA substrate at 4 °C. The preformed RT−DNA complex was mixed with 0.1 mM dCTP at 37 °C. For experiments with gp43exo$^-$, 100 nM gp43exo$^-$ was preincubated for 30 min with 400 nM DNA substrate at 4 °C prior to mixing with 0.1 mM dCTP at 25 °C. Reactions were carried out for various times, quenched with 0.5 M EDTA, and quantified as described (*20*). Product was separated by denaturing gel electrophoresis, imaged by PhosphorImager (Amersham Biosciences, Piscataway, NJ), and quantified by ImageQuant software. The time course of dCMP addition y was fit to

$$y = B \exp(-k_{obs}t) + k_{ss}t + C \quad (1)$$

where B is the burst amplitude, k_{obs} is the first-order rate constant for the burst phase, k_{ss} is the steady-state rate, t is time, and C is a constant.

For experiments as a function of RT concentration, 100−900 nM total RT was preincubated overnight with 500 or 1000 nM 25/36-mer and reacted with dCTP for periods of 1−10 s as above. The time course was fit by linear regression to

$$y = B + k_{ss}t \quad (2)$$

where B is the burst amplitude at $t = 0$ and k_{ss} is the steady-state rate.

(B) Single Nucleotide Addition with Trap. Single nucleotide addition experiments were done as in (A), except that the dCTP solution also contained 2 mg/mL heparin or salmon sperm DNA to bind free RT. The two traps gave identical results.

(C) Direct Mixing of RT and DNA Substrate. The amount of active enzyme present in RT solutions in the absence of DNA substrate was assayed by single nucleotide addition experiments, in which the RT−DNA complex was *not* preformed. RT (100−1000 nM total) was incubated overnight with 0.1 mM dCTP at 4 °C. This solution was mixed with 500 or 1000 nM 25/36-mer for periods of 1−10 s, and the results were analyzed as in (A) using eq 2.

(D) Trap-Chase. RT (700 nM total) was preincubated with 400 nM DNA substrate overnight at 4 °C. The preformed RT−DNA complex was mixed with 2 mg/mL heparin at 37 °C. For experiments with gp43exo$^-$, 100 nM gp43exo$^-$ was preincubated with 400 nM DNA substrate for 30 min at 4 °C prior to mixing with 2 mg/mL heparin at 25 °C. After incubation with trap for periods of 0.02−5 s, 0.1 mM dCTP was added, and the reaction was quenched 10 s later as in (A). The time course of dissociation of the polymerase−DNA complex was fit to an exponential function

$$y = A_1 \exp[-k_{off}(1)t] + A_2 \exp[-k_{off}(2)t\,] + C \quad (3)$$

[2] HIV-1 RT has been reported to have two burst phases followed by a linear steady-state phase (*32*). Under pseudo-first-order conditions, we and others (*9*−*11*) observe only one burst phase followed by a steady-state phase. The reason for this discrepancy is unclear, but may be due to the use of different DNA sequences and reaction conditions.

where A_i and $k_{off}(i)$ are amplitudes and dissociation rate constants and C is a constant.

(E) Fluorescence Stopped-Flow. The fluorescent guanine analogue 6-MI was substituted for guanosine at position 26 on the template strand of the 25/36-mer across from the incoming nucleotide. A fluorescence quantum yield of 0.10 was measured for 25/36-mer 6-MI in RT reaction buffer at 350 nm excitation wavelength, 25 °C, relative to quinine sulfate (*30*, *31*). The relative quantum yield of 2.5 μM 25/36-mer 6-MI at 37 °C decreased ~20% after overnight preincubation with 5 μM total RT at 4 °C. The ability of 25/36-mer 6-MI to serve as substrate was evaluated in single nucleotide addition experiments with dCTP, dATP, dGTP, or a mixture of all four dNTPs. Under the conditions in (A), RT did not extend the primer strand of 25/36-mer 6-MI.

Dissociation kinetics of the RT−DNA complex were monitored on a KinTek SF-2001 stopped-flow apparatus (State College, PA). RT (5 μM total) was preincubated with 2.5 μM 25/36-mer 6-MI DNA overnight at 4 °C in the absence and presence of 0.1 M dCTP. A 50 μL sample of the preformed RT−DNA or RT−DNA−dCTP complex was mixed with an equal volume of 2 mg/mL heparin at 37 °C, and the fluorescence was monitored as a function of time. The excitation wavelength was 350 nm. The Glans-Thompson excitation polarizer was set at 55°, and the emission polarizer was set at 90° to avoid anisotropic effects. A 400 nm cut-on filter was used to remove scattered excitation light. Experiments were performed using time scales of 0.25−8 s. Typically five traces were collected and averaged for each time scale. The time course of dissociation of the RT−25/36-mer 6-MI DNA complex was fit to eq 3 by global analysis of data for different time scales. In the global analysis, rate constants $k_{off}(i)$, but not amplitudes A_i, were assumed to be the same for all time scales.

(F) Simulations. Single nucleotide addition experiments were simulated using the KinFitSim 3.0.3 program from Kintek. The following values were taken from the literature: association rate constant of RT and DNA of 5×10^8 M^{-1} s^{-1} (*32*), pyrophosphorolysis rate constant $k_{pyro} = 160$ s^{-1} (*10*), dissociation constant of the RT−DNA−dCTP ternary complex K_D(dCTP) = 6 μM (*33*), and dissociation constants of the RT−DNA−PP_i ternary complex $K_D(PP_i)$ = 1.5 mM (*11*) and 7.2 mM (*10*). Initial substrate concentrations were 400 nM DNA and 0.1 mM dCTP. Initial enzyme concentrations were 300 nM total RT for simulations of single nucleotide addition experiments and 700 nM total RT for simulations of trap-chase experiments, corresponding to 70 and 260 nM active RT as estimated from gel mobility shift data.

Gel Mobility Shift Assay. The amount of DNA-bound RT present in solutions of the preformed RT−DNA complex in (A) was assayed by native gel electrophoresis. The 25/36-mer was labeled using [γ-^{33}P]ATP and T4 polynucleotide kinase. RT (0−900 nM total) was equilibrated with 1000 nM 25/36-mer in RT reaction buffer overnight at 4 °C. Reagent concentrations are final concentrations after 2-fold dilution prior to electrophoresis. Samples were loaded on a 4% polyacrylamide gel (3.25 × 0.4 in.) in 40 mM Tris−acetate, pH 8.0, and 1 mM EDTA. Gels were run at room temperature for 1 h (100 V constant voltage), dried on a Bio-Rad model 583 gel dryer (Hercules, CA), and quantified as described above. Discontinuity of sample and gel buffers caused severe streaking of the bands. To correct for this, the area of the unshifted band was estimated from the lane containing DNA alone, and the area between shifted and unshifted bands was counted as the shifted band. The percent DNA-bound RT was calculated assuming that the amount of DNA in the shifted band represented a 1:1 complex of RT dimer and 25/36-mer.

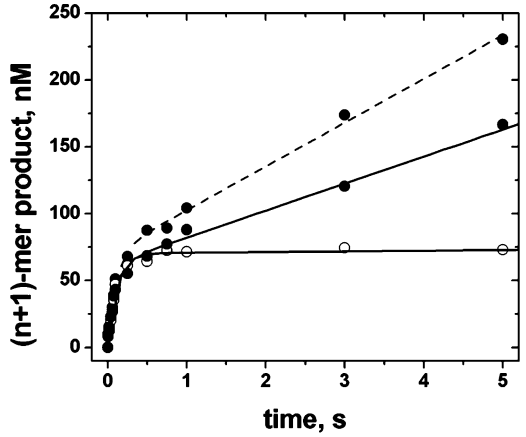

FIGURE 1: Time course of single nucleotide addition to random sequence DNA substrate. Final concentrations: 300 nM total RT and 400 nM 25/36-mer with 0.1 mM dCTP (●, —); 0.1 mM dCTP and 1 mg/mL BSA (●, - - -); 0.1 mM dCTP and 2 mg/mL salmon sperm DNA (○, —).

RESULTS

Burst Amplitudes for Random Sequence DNA Substrates. The 25/36-mer DNA substrate of random sequence is used as the control substrate for HIV-1 RT (Table 1). The 25/36-mer as well as the 34/62-mer random sequence and 30/60-mer EIAV DNA substrates were used in our previous study (*20*). Figure 1 shows a time course for single nucleotide addition of dCMP by RT with the typical rapid burst and linear phases (filled circles). The rate constants k_{obs} and k_{cat} in Table 2 are consistent with published values for random sequence DNA substrates (*9*, *10*). The burst amplitude B is only about 22% of $[RT]_{tot}$. Substoichiometric burst amplitudes are commonly observed in pre-steady-state kinetic studies of RT (*9*, *10*, *12*−*16*). To test whether the low burst amplitudes were due to loss of enzyme on surfaces of tubes and pipets used in the reaction, experiments were performed in RT reaction buffer containing 1 mg/mL BSA. The presence of BSA did not affect the burst amplitude, though it increased enzyme turnover slightly, perhaps by molecular crowding (Figure 1). Single nucleotide addition experiments using authentic RT indicate that the N-terminal His tags on both subunits of the p66/p51 heterodimer have no effect on the burst amplitude B or rate constants k_{obs} and k_{cat} (Table 2).

To test whether the low burst amplitudes were due to RT sliding on primer/template or binding in the opposite orientation at the 3′-OH of the template strand, two additional DNA substrates of random sequence were used (Table 1). The 34/62-mer substrate has longer double- and single-stranded regions to provide more binding sites compared to the 25/36-mer substrate (*20*). If RT slid along double- or single-stranded DNA, the burst amplitude should be lower for the 34/62-mer than 25/36-mer substrate. The 33/41-mer DNA substrate has most of the double-stranded region of

Table 2: Kinetic Parameters for Random Sequence DNA Substrates[a]

substrate	*B*, nM	% active[b]	k_{obs}, s^{-1}	k_{ss}, nM s^{-1}	k_{cat},[c] s^{-1}
		HIV-1 Reverse Transcriptase			
25/36-mer	67 ± 5	22 ± 2	14 ± 2	15.0 ± 0.6	0.22 ± 0.06
+1 mg/mL BSA	58 ± 3	19 ± 1	9 ± 1	20.0 ± 0.5	0.34 ± 0.03
+trap	65 ± 3	22 ± 1	8 ± 1	0.5 ± 0.4	0.008 ± 0.007
authentic RT[d]	60 ± 4	19 ± 1	13 ± 2	15.8 ± 0.7	0.26 ± 0.04
34/62-mer	63 ± 3	21 ± 1	17 ± 2	8.6 ± 0.4	0.14 ± 0.01
33/41-mer					
34-mer product	31 ± 2	10 ± 1	21 ± 3	8.4 ± 0.3	0.27 ± 0.01
42-mer product	40 ± 1	13.0 ± 0.3	23 ± 2	9.4 ± 0.2	0.23 ± 0.01
total	71 ± 3	23 ± 1			
		T4 DNA Polymerase Exo$^-$			
34/62-mer	94 ± 6	94 ± 6	14 ± 2	160 ± 8	1.7 ± 0.1

[a] Single nucleotide addition experiments using $[RT]_{tot} = 300$ nM or [gp43exo$^-$] = 100 nM. Errors are standard deviations for three experiments. [b] Calculated from $B/[pol]_{tot} \times 100$. [c] Calculated from $k_{cat} = k_{ss}/B$. [d] RT with no His tags.

the 34/62-mer and two template overhangs beginning with guanosine. One overhang has the same 11 nucleotides as the 25/36-mer, and the other has 3 nucleotides. If RT bound in two orientations on the 25/36-mer substrate, the total burst of 34- and 42-mer products using the 33/41-mer substrate should be higher than the burst of the 26-mer product, and the apparent percent active enzyme would increase. The results in Table 2 show that the availability of additional DNA binding sites and a second extendable 3′-OH does not affect the total burst amplitude or rate constants.

Small burst amplitudes were reported for HIV-1 RT using DNA substrates containing stable hairpin structures (*15*) or modified bases (*17*, *19*, *34*). Subsequent single nucleotide addition experiments using unlabeled primer/template to trap free RT clearly resolved two burst phases from normal and stalled forms of the RT−DNA complex, with the normal form converting to product more rapidly than the stalled form. To test whether the substoichiometric burst amplitudes in Table 2 were due to stalled RT−DNA complexes, trap experiments were performed with the 25/36-mer substrate (Figure 1). The time course showed a single rapid burst followed by a plateau (open circles) with burst amplitude *B* and rate constant k_{obs} similar to the values obtained in the absence of trap (Table 2). Clearly, the trapping agents do not interfere with the chemical step of the reaction but effectively sequester the active enzyme after a single turnover. The absence of a second burst phase in our experiments is consistent with the minimal kinetic mechanism in Scheme 1.

In contrast to RT, gp43exo$^-$ gives a stoichiometric burst amplitude on the 34/62-mer DNA substrate (Table 2). The rate constants k_{obs} and k_{cat} agree with published values for gp43exo$^-$ (*24*, *35*, *36*).

Concentration Dependence of Percent Active RT. Only dimeric forms of RT have catalytic activity (*2*). A simple explanation for loss of enzyme activity is subunit dissociation. If the RT solution contained an equilibrium mixture of monomers and dimers, then the percent active enzyme as well as the burst amplitude would increase at higher protein concentrations. To test this hypothesis, single nucleotide addition experiments were performed as a function of total RT concentration using constant amounts of the 25/36-mer DNA substrate. Figure 2 shows a hyperbolic increase in the percent active RT with increasing $[RT]_{tot}$. This observation strongly suggests that the substoichiometric burst amplitudes are due to reversible dissociation of the dimeric enzyme. It

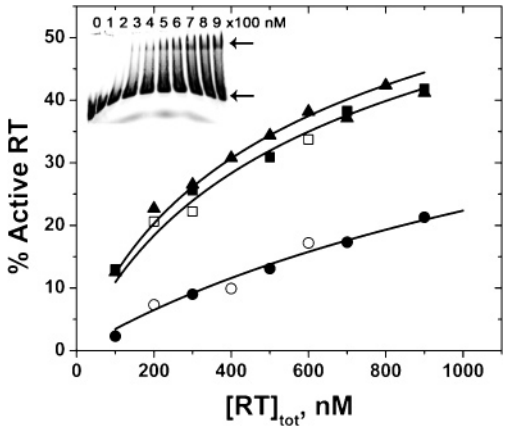

FIGURE 2: Dependence of percent active RT on total RT concentration. Preincubation (□, ■) and direct mixing (○, ●) of RT and 25/36-mer DNA substrate (500 nM, ○, □; 1000 nM, ●, ■) in single nucleotide addition experiments; percent active RT = $B/[RT]_{tot} \times 100$. Also shown is the dependence of percent DNA-bound RT on total RT concentration. Preincubation (▲) of RT and 1000 nM 25/36-mer DNA substrate in gel mobility shift assay. Lines are drawn to guide the eye. The inset is the gel image. Arrows indicate DNA (lower) and the RT−DNA complex (upper).

also suggests that the equilibrium dissociation constant K_d(p66/p51) of the heterodimer is considerably higher than the widely cited value of 0.4 nM (*37*).

The presence of DNA substrate during overnight preincubation perturbs the subunit equilibria by binding dimeric forms of RT. To measure the amount of active enzyme in the absence of DNA, single nucleotide addition experiments were performed as a function of total RT concentration by mixing RT and DNA solutions directly in the rapid-quench apparatus. Because dimer formation is a slow process (*38*), only dimeric enzyme present in the RT solution at the time of mixing will bind DNA substrate and catalyze dCMP incorporation. As seen in Figure 2, the percent active RT in direct mixing experiments is less than half that of preincubated experiments. At $[RT]_{tot} = 300$ nM, RT appears to be about 10% active without preincubation, 15% active with 30 min preincubation (not shown), and 25% active with overnight preincubation. The apparent dimerization constant for p66/p51 obtained by fitting the direct mixing data to a simple dissociation reaction p66/p51 = p66 + p51 is K_d(app) = 2.6 μM. However, this value must be taken as a rough estimate, because it was not measured under equilibrium conditions.

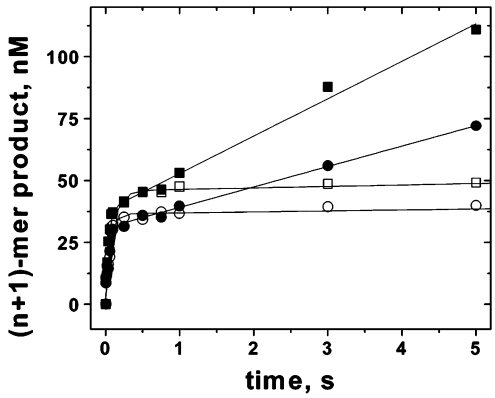

FIGURE 3: Time course of single nucleotide addition to CTS-containing DNA substrates. Final concentrations: 300 nM total RT and 400 nM 30/60-mer HIV (●, ○) or 30/60-mer EIAV (■, □) with 0.1 mM dCTP (●, ■); 0.1 mM dCTP and 2 mg/mL salmon sperm DNA (○, □).

RT binds tightly to DNA substrates with nanomolar affinities as measured by active site titration (*9*), gel mobility shift assay (*10*), and fluorescence (*39*). If only dimeric forms bind to DNA, then the percent DNA-bound RT would increase with protein concentration in parallel with percent active RT. To test this hypothesis, gel mobility shift assays were performed under the same conditions as the single nucleotide addition experiments with overnight preincubation. DNA binding should be essentially stoichiometric at the concentrations of RT and DNA substrate used in the experiments. Figure 2 shows that the percent DNA-bound RT from mobility shift data is about the same or slightly higher than the percent active RT from burst amplitude data. These results confirm that the substoichiometric burst amplitudes commonly observed for RT with random sequence DNA substrates are due primarily to the amount of dimeric RT present in the reaction mixture. Neither the p66 nor p51 subunit alone shifted DNA mobility at protein concentrations ≤ 2 μM, indicating that monomeric forms of RT do not bind DNA substrate (not shown). However, DNA mobility shifts were observed at higher protein concentrations where significant amounts of homodimer are expected.

Burst Amplitudes for CTS-Containing DNA Substrates. To test whether the HIV CTS sequence also causes a reduction in burst amplitude, single nucleotide addition experiments were performed using CTS-containing DNA substrates (Table 1). Like our previous substrates containing EIAV CTS sequences (*20*), 30/60-mer HIV has the position of single nucleotide addition one residue upstream of the CTS sequence. In the case of EIAV, this junction is located 6 and 16 nucleotides upstream of *ter*1 and *ter*2 on the EIAV genome (*40*). The analogous substrate for HIV locates the junction 5, 20, and 29 nucleotides away from *ter*0, *ter*1, and *ter*2 (*7*, *41*). Figure 3 shows time courses for single nucleotide addition of dCMP using 30/60-mer HIV and 30/60-mer EIAV for comparison. The rate constants k_{obs} and k_{cat} for CTS-containing substrates were in good agreement with those obtained for random sequence DNA substrates (Table 3). The absence of a second burst phase in the presence of trap is likewise consistent with the minimal kinetic mechanism (Scheme 1). The burst amplitudes were lower by a factor of 2 for both HIV and EIAV CTS-containing substrates, in accord with our previous results for EIAV CTS sequences (*20*). The importance of the upstream duplex sequence of the HIV CTS in lowering the burst amplitude was confirmed using the 33/41-mer HIV substrate (Table 1). This substrate has two extendable 3′-OH groups with the same double-stranded region as 30/60-mer HIV and the same two template overhangs as the random sequence 33/41-mer. The total burst amplitudes and the rate constants are similar to the values obtained for the 30/60-mer HIV substrate (Table 3). gp43exo$^-$ again gave a stoichiometric burst amplitude using the 30/60-mer HIV (Table 3) with the same rate constants as obtained for the 34/62-mer random sequence.

Dissociation Kinetics. To evaluate the effect of DNA sequence, the kinetics of dissociation of RT−DNA complexes were measured by two techniques: trap-chase rapid-quench and fluorescence stopped-flow. The former monitors the RT−DNA complex by dCMP incorporation and detects catalytically competent or productive complexes, whereas the latter monitors the RT−DNA complex by fluorescence and detects both productive and nonproductive complexes.

Trap-chase experiments were performed using the 25/36-mer, 30/60-mer HIV, and 30/60-mer EIAV substrates (Figure 4). The preincubated RT−DNA complex was mixed with heparin or salmon sperm DNA trap, which sequesters any RT not bound to labeled DNA substrate (Figures 1 and 3). After times ranging from 20 ms to 5 s, dCTP was added for 10 s to assay the amount of the RT−DNA complex remaining. For all substrates, the dissociation kinetics were fit to two exponential functions with a fast rate constant $k_{off}(1) \approx 20$ s^{-1} and a slow rate constant $k_{off}(2) \approx 0.2$ s^{-1} (Table 4). The fast rate constant $k_{off}(1)$ was unexpected. The slow rate constant $k_{off}(2) \approx k_{cat}$ is the expected value from single nucleotide addition experiments (Tables 2 and 3), in which dissociation of the D_{n+1} product from the $E{\cdot}D_{n+1}$ complex is believed to be the rate-limiting step of Scheme 1. These results indicate that there are two forms of the RT−DNA complex present in solution. The relative amplitudes of the two kinetic phases depend on DNA sequence (Table 4). The amplitude of the slow rate constant decreases from about 50% for random sequence DNA to about 30% for CTS-containing DNA.

Like the burst amplitude, the initial amplitude $A_1 + A_2$ of the decay curve reflects the amount of active RT present in solution. Comparing experiments with 25/36-mer and 700 nM RT, the percent active RT is about 32% from trap-chase data (Table 4) and 37% from burst amplitude data (Figure 2). The percent active RT estimated from the amount of product formed at the first time point ($t = 20$ ms) of the trap-chase experiment in Figure 4 is 28%. The initial amplitude decreases by a factor of 2 for CTS-containing DNA compared to random sequence DNA (Table 4), in parallel with the burst amplitudes (Tables 2 and 3). Within error, the trap-chase experiments account for all of the active RT in the single nucleotide addition experiments.

For comparison, trap-chase experiments were also performed with gp43exo$^-$ (Figure 4). The dissociation kinetics of the gp43exo$^-$−DNA complex were fit to one exponential function with $k_{off} = 2.3 \pm 0.2$ s^{-1}, in good agreement with k_{cat} from single nucleotide addition experiments (Tables 2 and 3). This is consistent with previous reports for the bacteriophage DNA polymerase reaction mechanism, in which release of the extended DNA product is the rate-limiting step (*24*, *35*).

Table 3: Kinetic Parameters for CTS-Containing DNA Substrates[a]

substrate	*B*, nM	% active[b]	k_{obs}, s^{-1}	k_{ss}, nM s^{-1}	k_{cat},[c] s^{-1}
		HIV-1 Reverse Transcriptase			
30/60-mer HIV	33 ± 2	11.0 ± 0.7	19 ± 5	7 ± 1	0.22 ± 0.05
+trap	30 ± 3	10 ± 1	16 ± 3	0.4 ± 0.4	0.008 ± 0.007
30/60-mer EIAV	41 ± 3	14 ± 1	19 ± 7	14.8 ± 0.8	0.36 ± 0.05
+trap	42 ± 3	14 ± 1	10 ± 1	0.6 ± 0.3	0.014 ± 0.008
33/41-mer HIV					
34-mer product	18 ± 1	6.0 ± 0.3	11 ± 1	7.9 ± 0.1	0.44 ± 0.01
42-mer product	16 ± 1	5.0 ± 0.3	13 ± 1	7.9 ± 0.2	0.16 ± 0.01
total	34 ± 2	11.0 ± 0.6			
		T4 DNA Polymerase Exo$^-$			
30/60-mer HIV	101 ± 8	101 ± 8	50 ± 10	180 ± 10	1.9 ± 0.1

[a] Single nucleotide addition experiments using $[RT]_{tot}$ = 300 nM or [gp43exo] = 100 nM. Errors are standard deviations for three experiments. [b] Calculated from $B/[pol]_{tot} \times 100$. [c] Calculated from $k_{cat} = k_{ss}/B$.

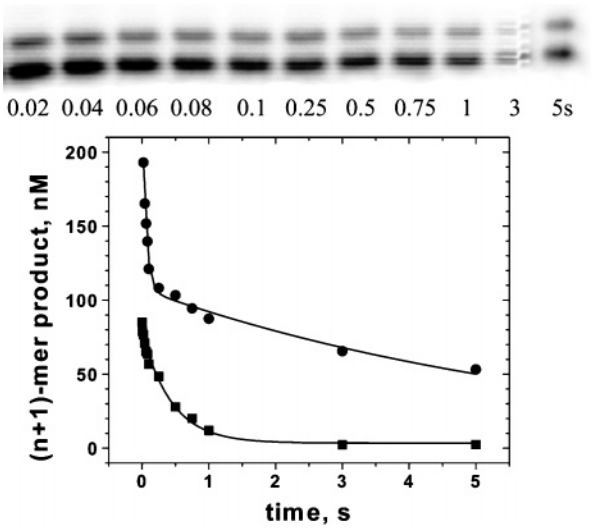

FIGURE 4: Dissociation of polymerase−DNA complexes in trap-chase rapid-quench experiments. The upper panel is the gel image of the RT−25/36-mer reaction showing 25-mer primer and 26-mer product. The lower panel is the PhosphorImager analysis of RT−25/36-mer (●) and gp43exo$^-$−30/60-mer HIV (■) reactions. Final concentrations: 700 nM total RT or 100 nM gp43exo$^-$, 400 nM DNA substrate, 0.1 mM dCTP, and 2 mg/mL heparin.

Fluorescence stopped-flow experiments were performed using 25/36-mer 6-MI DNA (Figure 5). Although the 6-MI base forms a Watson−Crick base pair with cytosine (*42*), it did not serve as template for polymerization. The inability of RT to incorporate a nucleotide opposite a template 6-MI precludes trap-chase measurements of dissociation of the RT−25/36-mer 6-MI complex but enables stopped-flow measurements in the absence and presence of dCTP. The absorption spectrum of 25/36-mer 6-MI has a peak at 350 nm, which allows selective excitation of the fluorescent base analogue in the presence of RT and DNA (*42*). The increase in fluorescence intensity upon dissociation of the RT−25/36-mer 6-MI complex after being mixed with trap was fit to two exponential functions. The rate constants $k_{off}(1)$ and $k_{off}(2)$ and relative amplitudes of the two kinetic phases from the stopped-flow data agree with the values for unsubstituted 25/36-mer DNA measured by trap-chase (Table 4). dCTP (0.1 mM) had no effect on the dissociation kinetics. This is consistent with the ordered mechanism in Scheme 1, in which dNTP substrate dissociates from RT before DNA substrate in the absence of catalysis and dNTP binding to the RT−DNA complex is a rapid equilibrium (*10*). Dissociation of the binary RT−DNA complex is the rate-limiting step, so that the binary and ternary complexes have the same apparent dissociation rates.

The fact that trap-chase and stopped-flow experiments give the same dissociation kinetics means that (I) the two forms of the RT−DNA complex are both productive or (II) the two forms, one productive and one nonproductive, interconvert on the time scale of polymerization. In case Ia with two productive forms of the RT−DNA complex that do not interconvert, the dissociation kinetics are given by two exponential functions in eq 3. The dissociation rate constants and relative amounts of the two complexes are given by the values in Table 4. If the association rate constants of the two complexes were the same, the 100-fold difference in dissociation rate constants $k_{off}(1)$ and $k_{off}(2)$ would translate to a 100-fold difference in DNA binding affinity. In case Ib with two productive forms that interconvert or in case II, the dissociation kinetics are more complicated. Scheme 2 gives the kinetic mechanism for irreversible dissociation of two interconverting forms of the RT−DNA complex in the presence of trap, as in the trap-chase and stopped-flow experiments. For consistency with Scheme 3, the two forms are called productive p and nonproductive n.[3]

Scheme 2: Dissociation Kinetics of RT−DNA Complex

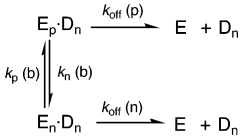

where $E_{p,n}$ are productive and nonproductive forms of DNA-bound RT, $k_{off}(p)$ and $k_{off}(n)$ are dissociation rate constants for productive and nonproductive complexes, $k_n(b)$ is the rate constant for conversion of productive to nonproductive complex, and $k_p(b)$ is the rate constant for conversion of nonproductive to productive complex. The dissociation kinetics of the two interconverting forms are given by two coupled differential equations

$$dE_p{\cdot}D_n/dt = -[k_{off}(p) + k_n(b)]E_p{\cdot}D_n + k_p(b)E_n{\cdot}D_n \quad (4a)$$

$$dE_n{\cdot}D_n/dt = k_n(b)E_p{\cdot}D_n - [k_{off}(n) + k_p(b)]E_n{\cdot}D_n \quad (4b)$$

[3] Scheme 2 and eqs 4a,b are symmetric, so assignment of a pair of rate constants to a form of the RT−DNA complex is arbitrary.

Table 4: Dissociation Kinetics of the RT−DNA Complex[a]

substrate	A_1, nm	rel A_1[b]	$k_{off}(1)$, s^{-1}	A_2, nm	rel A_2[b]	$k_{off}(2)$, s^{-1}
			HIV-1 Reverse Transcriptase[c]			
25/36-mer[d]	122 ± 8	0.53 ± 0.03	17 ± 2	107 ± 3	0.47 ± 0.01	0.15 ± 0.02
25/36-mer 6-MI[e]		0.47 ± 0.03	22		0.53 ± 0.03	0.58
+dCTP[e]		0.46 ± 0.03	15		0.54 ± 0.03	0.50
30/60-mer HIV[d]	82 ± 6	0.68 ± 0.09	18 ± 3	39 ± 4	0.32 ± 0.04	0.26 ± 0.07
30/60-mer EIAV[d]	86 ± 6	0.68 ± 0.07	17 ± 3	41 ± 3	0.32 ± 0.03	0.27 ± 0.07
			T4 DNA Polymerase Exo$^-$[f]			
30/60-mer HIV[d]	75 ± 3	1.0	2.3 ± 0.2			

[a] Data fit to biexponential function. [b] $A_1 + A_2 = 1$. [c] Trap-chase using $[RT]_{tot} = 700$ nM; stopped-flow using $[RT]_{tot} = 5$ μM. [d] Errors are standard deviations for two trap-chase experiments. [e] Global analysis of stopped-flow data on eight time scales. Errors are standard deviations. [f] Trap-chase using [gp43exo$^-$] = 100 nM.

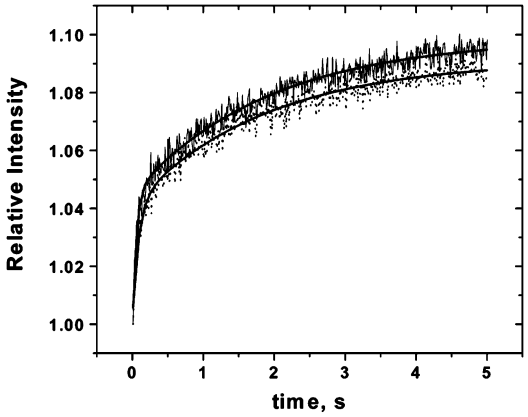

FIGURE 5: Dissociation of the RT−25/36-mer 6-MI complex in fluorescence stopped-flow experiments in the absence (—) and presence (···) of 0.1 mM dCTP. Final concentrations: 5 μM total RT, 2.5 μM 25/36-mer 6-MI, and 2 mg/mL heparin.

The decay of $E{\cdot}D_n(t) = E_p{\cdot}D_n(t) + E_n{\cdot}D_n(t)$ measured in the experiments has two exponential terms with preexponentials and decay rates that depend on all four rate constants (see Supporting Information). We estimated these four rate constants by comparing simulated and experimental decay curves for random sequence and CTS-containing DNA (Table 5). Initial concentrations of $E_p{\cdot}D_n(0)$ and $E_n{\cdot}D_n(0)$ were calculated from the equilibrium constant for conversion of productive to nonproductive complex $K_n(b) = k_n(b)/k_p(b)$ and the concentration of active RT in the trap-chase experiment. The dissociation rates of the two complexes were essentially independent of DNA sequence: $k_{off}(p) = 0.26$ s^{-1} and $k_{off}(n) = 0.08$ s^{-1} for the 25/36-mer and $k_{off}(p) = 0.24-0.26$ s^{-1} and $k_{off}(n) = 0.11-0.12$ s^{-1} for the CTS-containing DNAs. The k_{off} values for productive and nonproductive complexes differ by factors of 2−3, consistent with a small difference in DNA binding affinity. This is supported by the close agreement of burst amplitude and gel shift data (Figure 2). In contrast, the partitioning between productive and nonproductive complexes was sequence dependent. For the 25/36-mer, the interconversion rates were $k_p(b) = 25$ s^{-1} and $k_n(b) = 13.5$ s^{-1}; $K_n(b) = E_n{\cdot}D_n/E_p{\cdot}D_n = 0.54$ favors the productive complex. For the CTS-containing DNAs, $k_p(b) = 4.5-5$ s^{-1} and $k_n(b) = 13.5$ s^{-1}; $K_n(b) = 2.7-3$ favors the nonproductive complex.

Table 5: Kinetic Parameters for the Modified Mechanism[a]

	25/36-mer	25/36-mer	30/60-mer HIV	30/60-mer EIAV
		Dissociation Kinetics[b]		
	trap-chase	stopped-flow	trap-chase	trap-chase
$k_{off}(p)$, s^{-1}	0.26	0.28	0.26	0.24
$k_{off}(n)$, s^{-1}	0.08	0.07	0.12	0.11
$k_p(b)$, s^{-1}	25	22	4.5	5
$k_n(b)$, s^{-1}	13.5	14	13.5	13.5
$K_n(b) = k_n(b)/k_p(b)$	0.54	0.64	3.0	2.7
$E_p{\cdot}D_n(0)$, fraction	0.65	0.61	0.25	0.27
$E_n{\cdot}D_n(0)$, fraction	0.35	0.39	0.75	0.73
		Single Nucleotide Addition[c]		
$k_p(t)$, s^{-1}	0.5	0.4	0.12	0.1
$k_n(t)$, s^{-1}	3	3	1	1
$K_n(t) = k_n(t)/k_p(t)$	6.0	7.5	8.3	10
$E_p{\cdot}D_n{\cdot}$dNTP, fraction	0.14	0.12	0.11	0.09
$E_n{\cdot}D_n{\cdot}$dNTP, fraction	0.86	0.88	0.89	0.91

[a] Interconverting productive and nonproductive forms of RT−DNA and RT−DNA−dNTP complexes. [b] Data fit to Scheme 2. [c] Data fit to Scheme 3, using dissociation kinetics parameters from trap-chase and stopped-flow data.

DISCUSSION

Despite extensive study of HIV-1 RT, the consequences of the reversible subunit equilibria for solution studies of the enzyme have been largely ignored. Substoichiometric bursts of product formation are commonly reported for normal substrates (*9*, *10*, *13*−*16*). Explanations proffered for this phenomenon include dead enzyme, errors in protein concentration, or catalytically incompetent forms of the RT−DNA complex (*17*, *18*). RT concentration is usually determined from absorbance at 280 nm. We measured the extinction coefficient of the RT heterodimer by quantitative amino acid analysis and obtained $\epsilon(280) = (2.6 \pm 0.2) \times 10^5$ M^{-1} cm^{-1}, in good agreement with a previous determination of $\epsilon(280) = 2.99 \times 10^5$ M^{-1} cm^{-1} (*10*) as well as calculated values based on amino acid composition. None of these values agree with a much higher value of $\epsilon(280) = 5.20 \times 10^5$ M^{-1} cm^{-1} (*18*). In the absence of a UV-absorbing cofactor, experimental and calculated values of protein extinction coefficients usually agree within 10%. The RT heterodimer contains 37 tryptophans, which contribute about 80% of the absorbance at 280 nm. The extinction coefficient of the indole chromophore varies little with environment (*43*). The results presented here provide compelling evidence that monomeric forms of RT, which do not bind to DNA, account for partially inactive RT preparations. Because the dimerization reaction is slow (*38*, *44*), dimer concentrations may not reach equilibrium in a typical assay, which is performed without long preincubation. We surmise that differences in concentration of RT stock solutions and subsequent handling

Scheme 3: Modified Kinetic Mechanism of DNA Polymerization Catalyzed by HIV-1 RT

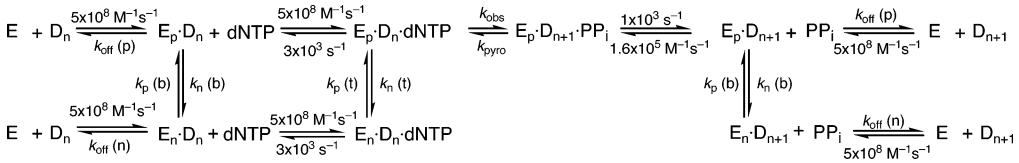

of dilutions account for much of the reported variation in enzyme activity with normal substrates. Consequently, all experiments reported here were performed using a 10 μM stock solution and uniform procedures to ensure the same dimer concentration at a given total RT concentration.

Although subunit dissociation may explain the substoichiometric burst amplitudes on random sequence DNA substrates, it does not account for sequence dependence of the burst amplitudes. Time courses of single nucleotide addition using both random sequence and CTS-containing DNA substrates are consistent with the minimal kinetic mechanism in Scheme 1 (Figures 1 and 3). The burst rate constant k_{obs} of 15 ± 5 s^{-1} is essentially independent of DNA sequence (Tables 2 and 3). This value is lower than our previous values of 56 ± 11 and 41 ± 4 s^{-1} using 0.1 mM dCTP (*20*) as well as the maximum rate $k_{pol} = 71$ s^{-1} for correct dCMP addition (*33*). The slower burst rate constant reported here likely reflects differences in buffer composition and pH.[4]

For the mechanism of DNA polymerization using random sequence and CTS-containing DNA substrates to be the same as Scheme 1, the dissociation rate, k_{off}, of the RT−DNA complexes should be independent of DNA sequence and equal to k_{cat}, the turnover number for RT. The biphasic dissociation kinetics, whether monitored by trap-chase rapid-quench or fluorescence stopped-flow, clearly indicate that the RT−DNA complex is a mixture of two forms. To our knowledge, biphasic dissociation kinetics have not been reported previously for RT or other DNA polymerases. We were able to resolve the fast rate constant by taking multiple data points at very early times (<100 ms) after addition of trap. The kinetic mechanism must be modified to accommodate parallel dissociation pathways of the two forms of the binary RT−DNA complex and possibly also the ternary RT−DNA−dNTP complex. For case Ia with two productive forms of the RT−DNA complex that do not interconvert, simulations of several parallel mechanisms for single nucleotide addition show that the steady-state rate would be governed by the fast dissociation rate $k_{off}(1)$, making k_{ss} 5−8-fold greater than the values in Tables 2 and 3. Because our data are not consistent with such a mechanism, we consider parallel dissociation pathways of two interconverting forms of the RT−DNA complex.

Simulations of a variety of parallel mechanisms for single nucleotide addition were carried out to test whether partitioning between two forms of binary and ternary complexes could affect the burst amplitude. The estimates of dissociation and interconversion rates in Table 5 were used in the simulations along with experimental and literature values of other rate constants. Here too, initial concentrations of the two forms were calculated using $K_n(b)$. Completely parallel reaction paths for the two forms reproduced the time course of single nucleotide addition for the 25/36-mer with the observed values of *B*, k_{obs}, and k_{ss} but failed to give a reduced burst amplitude for CTS-containing DNA. Accordingly, Scheme 3 shows equilibria between productive and nonproductive forms, with only the productive form undergoing the conformational change in the ternary complex prior to nucleotide addition (*9*, *10*). If the ternary complex is omitted from the mechanism, the burst amplitudes are too high for both 25/36-mer and CTS-containing DNA.

The sequence dependence of the burst amplitude can be simulated using Scheme 3 with the interconversion rate constants of the ternary complex, $k_p(t)$ and $k_n(t)$, as sole adjustable parameters (Table 5). The interconversion rates of the ternary complex must be slower than the chemical step, and the actual values mostly affect the simulated steady-state rate. The equilibrium constant $K_n(t) = k_n(t)/k_p(t)$ favors the nonproductive form for both the 25/36-mer and CTS-containing DNA. Scheme 2 is symmetric with respect to the two enzyme forms, whereas Scheme 3 has only one form that can catalyze nucleotide addition. If we reverse the names of the two forms, so that the productive form has the slower dissociation rate, then the simulated steady-state rate is too slow. While the proposed mechanisms in Schemes 2 and 3 are speculative and the estimated rate constants are probably not unique, the simulations demonstrate that dependence of burst amplitudes on DNA sequence may arise from modest sequence-dependent effects on the interconversion rates of two forms of binary and ternary complexes.

The mechanism of polymerization catalyzed by RT is similar to other DNA polymerases (*45*). As depicted in Scheme 1, the pathway begins with the binding of RT to DNA substrate followed by binding of Mg-dNTP to the RT−DNA complex. The enzyme then undergoes a conformational change that is required for efficient phosphoryl transfer. After formation of the chemical bond, pyrophosphate is released followed by translocation of the elongated DNA to the next template position. Extensive biochemical and structural studies of RT have provided insight into each step of this multistep pathway, encompassing formation of the initial RT−DNA complex (*6*) to enzyme forms that exist after phosphoryl transfer (*46*). Although the translocation step is kinetically invisible, recent structures of RT bound to chain-terminated DNA (*47*) and cross-linked to DNA (*48*) have provided unique information regarding this process. These structures show two distinct sites on the enzyme where primer/template can reside, named "P-site" and "N-site". Upon initial binding, the 3′-primer is positioned at the P-site and the N-site is temporarily unoccupied. Binding of dNTP occurs near the N-site to form the "open" ternary complex. This is followed by the aforementioned conformational change to form the "closed" ternary complex required for phosphoryl transfer. At this stage of the reaction cycle, both sites are occupied so that RT can dissociate during distributive DNA

[4] The pH of RT reaction buffer used previously (*20*) was slightly above 7.8. It was prepared from concentrated stock solutions of components without final adjustment of pH.

synthesis or translocate to the next primer position during processive replication.

Two distinct RT−DNA complexes were also recently detected in solution using multiparameter single-molecule fluorescence spectroscopy (*49*). The proposed structures differ by one nucleotide in the position of primer/template on RT. The 3′-primer is positioned at the P-site in one complex, but occupies the N-site in the other complex. Alternatively, the small structural difference in the complexes could be explained by movement of the thumb subdomain, as noted in crystal structures of RT (*6*, *46*, *50*, *51*).

We argue that the biphasic dissociation curves observed in the trap-chase and stopped-flow experiments represent RT−DNA complexes corresponding to primer/template bound in both the P- and N-sites of RT. Moreover, there is a distinct correlation between the relative amounts of each enzyme form during dissociation that track along with the burst amplitudes measured in single nucleotide addition experiments. We propose that the productive and nonproductive forms $E_{p,n}$ of DNA-bound RT in Schemes 2 and 3 are the P- and N-site complexes. The change in burst amplitudes as a function of nucleic acid sequence arguably reflects the relative population of P- and N-complexes. This statement can be justified if one considers that partitioning of primer/template between the P- and N-sites is reversible (*52*). Furthermore, the equilibrium between the two sites can be influenced by the physical properties of the chain terminator present at the 3′-primer (*52*). Our data showing variations in burst amplitudes using DNA substrates with or without a CTS region strongly suggest that partitioning of primer/template between sites on RT can also be influenced by DNA sequence. This may occur because the CTS is reported to possess a higher degree of curvature compared to DNA of random sequence (*41*). The attenuation of the polymerization activity when RT encounters the CTS could reflect partitioning of the primer/template into the N-site such that the binding of the next correct dNTP is highly disfavored. This is of particular importance since pyrophosphorolysis is reported to occur only when the 3′-primer is positioned in the N-site (*53*). Evaluation of whether CTS sequences enhance pyrophosphorolysis due to increased partitioning of the 3′-primer in the N-site will be of great interest.

It is especially relevant that the dissociation kinetics of the gp43exo$^-$−DNA complex differ from those of the RT−DNA complex. Specifically, the bacteriophage DNA polymerase displays a single exponential decay curve for dissociation of DNA in the absence and presence of the CTS region. Likewise, the burst amplitudes in single nucleotide addition experiments of this enzyme are unaffected by the CTS. The most straightforward explanation is that in gp43 the equilibrium between P- and N-complexes strongly favors the P-complex (*54*). However, it is still possible that RT and gp43 may share a similar mechanism in the intramolecular partitioning of primer/template on the enzyme, because gp43 possesses two distinct active sites, the polymerase and the exonuclease domain, in which DNA can reside (*55*). Although gp43 can partition the 3′-primer between these active sites, the equilibrium position of gp43 while bound to undamaged DNA lies far in the direction of the polymerase active site (*35*). Since the dissociation kinetics as well as burst amplitudes are unaffected by the CTS, the partitioning of primer/template between the polymerase and exonuclease domain of gp43 must be insensitive to sequence context. Indeed, this is predicted for replicative DNA polymerases capable of processive DNA synthesis for more than 10 kb in a single replicative pass.

SUPPORTING INFORMATION AVAILABLE

Equations describing the dissociation kinetics of the RT−DNA complex. This material is available free of charge via the Internet at http://pubs.acs.org.

REFERENCES

1. di Marzo Veronese, F., Copeland, T. D., DeVico, A. L., Rahman, R., Oroszlan, S., Gallo, R. C., and Sarngadharan, M. G. (1986) Characterization of highly immunogenic p66/p51 as the reverse transcriptase of HTLV−III/LAV, *Science 231*, 1289−1291.
2. Restle, T., Müller, B., and Goody, R. S. (1990) Dimerization of human immunodeficiency virus type 1 reverse transcriptase, *J. Biol. Chem. 265*, 8986−8988.
3. Restle, T., Müller, B., and Goody, R. S. (1992) RNase H activity of HIV reverse transcriptase is confined exclusively to the dimeric forms, *FEBS Lett. 300*, 97−100.
4. Bavand, M. R., Wagner, R., and Richmond, T. J. (1993) HIV-1 reverse transcriptase: polymerization properties of the p51 homodimer compared to the p66/p51 heterodimer, *Biochemistry 32*, 10543−10552.
5. Le Grice, S. F. J., Naas, T., Wohlgensinger, B., and Schatz, O. (1991) Subunit-selective mutagenesis indicates minimal polymerase activity in heterodimer-associated p51 HIV-1 reverse transcriptase, *EMBO J. 10*, 3905−3911.
6. Jacobo-Molina, A., Ding, J., Nanni, R. G., Clark, A. D., Jr., Lu, X., Tantillo, C., Williams, R. L., Kamer, G., Ferris, A. L., Clark, P., Hizi, A., Hughes, S. H., and Arnold, E. (1993) Crystal structure of human immunodeficiency virus type 1 reverse transcriptase complexed with double-stranded DNA at 3.0 Å resolution shows bent DNA, *Proc. Natl. Acad. Sci. U.S.A. 90*, 6320−6324.
7. Charneau, P., Mirambeau, G., Roux, P., Paulous, S., Buc, H., and Clavel, F. (1994) HIV-1 reverse transcription. A termination step at the center of the genome, *J. Mol. Biol. 241*, 641−662.
8. Majumdar, C., Abbots, J., Broder, S., and Wilson, S. H. (1988) Studies on the mechanism of human immunodeficiency virus reverse transcriptase, *J. Biol. Chem. 263*, 15657−15665.
9. Kati, W. M., Johnson, K. A., Jerva, L. F., and Anderson, K. S. (1992) Mechanism and fidelity of HIV reverse transcriptase, *J. Biol. Chem. 267*, 25988−25997.
10. Hsieh, J.-C., Zinnen, S., and Modrich, P. (1993) Kinetic mechanism of the DNA-dependent DNA polymerase activity of human immunodeficiency virus reverse transcriptase, *J. Biol. Chem. 268*, 24607−24613.
11. Reardon, J. E. (1993) Human immunodeficiency virus reverse transcriptase. A kinetic analysis of RNA-dependent and DNA-dependent DNA polymerization, *J. Biol. Chem. 268*, 8743−8751.
12. Spence, R. A., Anderson, K. S., and Johnson, K. A. (1996) HIV-1 reverse transcriptase resistance to nonnucleoside inhibitors, *Biochemistry 35*, 1054−1063.
13. Furge, L. L., and Guengerich, F. P. (1997) Analysis of nucleotide insertion and extension at 8-oxo-7,8-dihydroguanine by replicative T7 polymerase exo$^-$ and human immunodeficiency virus-1 reverse transcriptase using steady-state and pre-steady-state kinetics, *Biochemistry 36*, 6475−6487.
14. Cameron, C. E., Ghosh, M., Le Grice, S. F. J., and Benkovic, S. J. (1997) Mutations in HIV reverse transcriptase which alter RNase H activity and decrease strand transfer efficiency are suppressed by HIV nucleocapsid protein, *Proc. Natl. Acad. Sci. U.S.A. 94*, 6700−6705.
15. Suo, Z., and Johnson, K. A. (1998) DNA secondary structure effects on DNA synthesis catalyzed by HIV-1 reverse transcriptase, *J. Biol. Chem. 273*, 27259−27267.
16. Weiss, K. K., Bambara, R. A., and Kim, B. (2002) Mechanistic role of residue Gln^{151} in error prone DNA symthesis by human immunodeficiency virus type 1 (HIV-1) reverse transcriptase (RT), *J. Biol. Chem. 277*, 22662−22669.

17. Suo, Z., Lippard, S. J., and Johnson, K. A. (1999) Single d(GpG)/*cis*-diammineplatinum(II) adduct-induced inhibition of DNA polymerization, *Biochemistry 38*, 715−726.
18. Furge, L. L., and Guengerich, F. P. (1999) Explanation of pre-steady-state kinetics and decreased burst amplitude of HIV-1 reverse transcriptase at sites of modified DNA bases with an additional, non-productive enzyme-DNA-nucleotide complex, *Biochemistry 38*, 4818−4825.
19. Woodside, A. M., and Guengerich, F. P. (2002) Effect of the O6 substituent on misincorporation kinetics catalyzed by DNA polymerases at O^6-methylguanine and O^6-benzylguanine, *Biochemistry 41*, 1027−1038.
20. Berdis, A. J., Stetor, S. R., Le Grice, S. F. J., and Barkley, M. D. (2001) Molecular mechanism of sequence-specific termination of lentiviral replication, *Biochemistry 40*, 12140−12149.
21. Le Grice, S. F. J., Cameron, C. E., and Benkovic, S. J. (1995) Purification and characterization of human immunodeficiency virus type 1 reverse transcriptase, *Methods Enzymol. 262*, 130−144.
22. Fasman, G. D. (1989) *Practical Handbook of Biochemistry and Molecular Biology*, CRC Press, Boca Raton, FL.
23. Gill, S. C., and von Hippel, P. H. (1989) Calculation of protein extinction coefficients from amino acid sequence data, *Anal. Biochem. 182*, 319−326.
24. Frey, M. W., Nossal, N. G., Capson, T. L., and Benkovic, S. J. (1993) Construction and characterization of a bacteriophage T4 DNA polymerase deficient in 3′→5′ exonuclease activity, *Proc. Natl. Acad. Sci. U.S.A. 90*, 2579−2583.
25. Rush, J., and Konigsberg, W. H. (1989) Rapid purification of overexpressed T4 DNA polymerase, *Prep. Biochem. 19*, 329−340.
26. Wong, I., Patel, S. S., and Johnson, K. A. (1991) An induced-fit kinetic mechanism for DNA replication fidelity: Direct measurement by single-turnover kinetics, *Biochemistry 30*, 526−537.
27. Kallansrud, G., and Ward, B. (1996) A comparison of measured and calculated single- and double-stranded oligodeoxynucleotide extinction coefficients, *Anal. Biochem. 236*, 134−138.
28. Kuchta, R. D., Mizrahi, V., Benkovic, P. A., Johnson, K. A., and Benkovic, S. J. (1987) Kinetic mechanism of DNA polymerase I (Klenow), *Biochemistry 26*, 8410−8417.
29. Johnson, K. A. (1986) Rapid kinetic analysis of mechanochemical adenosine triphosphatases, *Methods Enzymol. 134*, 677−705.
30. Liu, B., Barkley, M. D., Morales, G. A., McLaughlin, M. L., and Callis, P. R. (2000) Fluorescence properties of benz[*f*]indole, a wavelength and quenching selective tryptophan analog, *J. Phys. Chem. B 104*, 1837−1843.
31. Melhuish, W. H. (1961) Quantum efficiencies of fluorescence of organic substances: effect of solvent and concentration of the fluorescent solute, *J. Phys. Chem. 65*, 229−235.
32. Wöhrl, B. M., Krebs, R., Goody, R. S., and Restle, T. (1999) Refined model for primer/template binding by HIV-1 reverse transcriptase: pre-steady-state kinetic analyses of primer/template binding and nucleotide incorporation events distinguish between different binding modes depending on the nature of the nucleic acid substrate, *J. Mol. Biol. 292*, 333−344.
33. Zinnen, S., Hsieh, J.-C., and Modrich, P. (1994) Misincorporation and mispaired primer extension by human immunodeficiency virus reverse transcriptase, *J. Biol. Chem. 269*, 24195−24202.
34. Woodside, A. M., and Guengerich, F. P. (2002) Misincorporation and stalling at O^6-methylguanine and O^6-benzylguanine: evidence for inactive polymerase complexes, *Biochemistry 41*, 1039−1050.
35. Capson, T. L., Peliska, J. A., Kaboord, B. F., Frey, M. W., Lively, C., Dahlberg, M., and Benkovic, S. J. (1992) Kinetic characterization of the polymerase and exonuclease activities of the gene 43 protein of bacteriophage T4, *Biochemistry 31*, 10984−10994.
36. Berdis, A. J. (2001) Dynamics of translesion DNA synthesis catalyzed by the bacteriophage T4 exonuclease-deficient DNA polymerase, *Biochemistry 40*, 7180−7191.
37. Divita, G., Rittinger, K., Restle, T., Immendörfer, U., and Goody, R. S. (1995) Conformational stability of dimeric HIV-1 and HIV-2 reverse transcriptases, *Biochemistry 34*, 16337−16346.
38. Divita, G., Rittinger, K., Geourjon, C., Deléage, G., and Goody, R. S. (1995) Dimerization kinetics of HIV-1 and HIV-2 reverse transcriptase: a two step process, *J. Mol. Biol. 245*, 508−521.
39. Divita, G., Müller, B., Immendorfer, U., Gautel, M., Rittinger, K., Restle, T., and Goody, R. S. (1993) Kinetics of interaction of HIV reverse transcriptase with primer/template, *Biochemistry 32*, 7966−7971.
40. Stetor, S. R., Rausch, J. W., Guo, M.-J., Burnham, J. P., Boone, L. R., Waring, M. J., and Le Grice, S. F. J. (1999) Characterization of (+) strand initiation and termination sequences located at the center of the equine infectious anemia virus genome, *Biochemistry 38*, 3656−3667.
41. Lavigne, M., Roux, P., Buc, H., and Schaeffer, F. (1997) DNA curvature controls termination of plus strand DNA synthesis at the centre of HIV-1 genome, *J. Mol. Biol. 266*, 507−524.
42. Hawkins, M. E., Pfleiderer, W., Balis, F. M., Porter, D., and Knutson, J. R. (1997) Fluorescence properties of pteridine nucleoside analogs as monomers and incorporated into oligonucleotides, *Anal. Biochem. 244*, 86−95.
43. Strickland, E. H., and Billups, C. (1973) Oscillator strengths of the ^1L_a and ^1L_b absorption bands of tryptophan and several other indoles, *Biopolymers 12*, 1989−1995.
44. Wöhrl, B. M., Krebs, R., Thrall, S. H., Le Grice, S. F. J., Scheidig, A. J., and Goody, R. S. (1997) Kinetic analysis of four HIV-1 reverse transcriptase enzymes mutated in the primer grip region of p66, *J. Biol. Chem. 272*, 17581−17587.
45. Brautigam, C. A., and Steitz, T. A. (1998) Structural and functional insights provided by crystal structures of DNA polymerases and their substrate complexes, *Curr. Opin. Struct. Biol. 8*, 54−63.
46. Huang, H., Chopra, R., Verdine, G., and Harrison, S. C. (1998) Structure of a covalently trapped catalytic complex of HIV-1 reverse transcriptase: implications for drug resistance, *Science 282*, 1669−675.
47. Sarafinos, S. G., Clark, A. D., Jr., Das, K., Tuske, S., Birktoft, J. J., Ilankumaran, P., Ramesha, A. R., Sayer, J. M., Jerina, D. M., Boyer, P. L., Hughes, S. H., and Arnold, E. (2002) Structures of HIV-1 reverse transcriptase with pre- and post-translation AZTMP-terminated DNA, *EMBO J. 21*, 6614−6624.
48. Sarafinos, S. G., Clark, A. D., Jr., Tuske, S., Squire, C. J., Das, K., Sheng, D., Ilankumaran, P., Remesha, A. R., Kroth, H., Sayers, J. M., Jerina, D. M., Boyer, P. L., Hughes, S. H., and Arnold, E. (2003) Trapping HIV-1 reverse transcriptase before and after translocation on DNA, *J. Biol. Chem. 278*, 16280−16288.
49. Rothwell, P. J., Berger, S., Kensch, O., Felekyan, S., Antonik, M., Wöhrl, B. M., Restle, T., Goody, R. S., and Seidel, C. A. M. (2003) Multiparameter single-molecule fluorescence spectroscopy reveals heterogeneity of HIV-1 reverse transcriptase:primer/template complexes, *Proc. Natl. Acad. Sci. U.S.A. 100*, 1655−1660.
50. Hsiou, Y., Ding, J., Das, K., Clark, A. D., Jr., Hughes, S. H., and Arnold, E. (1996) Structure of unliganded HIV-1 reverse transcriptase at 2.7 Å resolution: implications of conformational changes for polymerization and inhibition mechanisms, *Structure 4*, 853−857.
51. Sarafianos, S. G., Das, K., Ding, J., Boyer, P. L., Hughes, S. H., and Arnold, E. (1999) Touching the heart of HIV-1 drug resistance: the fingers close down on the dNTP at the polymerase active site, *Chem. Biol. 6*, R137−R146.
52. Marchand, B., and Götte, M. (2003) Site-specific footprinting reveals differences in the translocation status of HIV-1 reverse transcriptase, *J. Biol. Chem. 278*, 35362−35372.
53. Boyer, P. L., Sarafinos, S. G., Arnold, E., and Hughes, S. H. (2001) Nucleoside analog resistance casued by insertions in the fingers of human immunodeficiency virus type 1 reverse transcriptase involves ATP-mediated excision, *J. Virol. 76*, 9143−9151.
54. Franklin, M. C., Wang, J., and Steitz, T. A. (2001) Structure of the replicating complex of a pol alpha family DNA polymerase, *Cell 105*, 657−667.
55. Spicer, E. K., Rush, J., Fung, C., Reha-Krantz, L. J., Karam, J. D., and Konigsberg, W. H. (1988) Primary structure of T4 DNA polymerase. Evolutionary relatedness to eucaryotic and other procaryotic DNA polymerases, *J. Biol. Chem. 263*, 7478−7486.

BI048000P